Available online at www.sciencedirect.com
ScienceDirect
Journal of Sound and Vibration 318 (2008) 131–147
JOURNAL OF SOUND AND VIBRATION
www.elsevier.com/locate/jsvi

Dynamic identification of beam axial loads using one flexural mode shape

Nerio Tullini, Ferdinando Laudiero*

Department of Engineering, University of Ferrara, Via Saragat 1, 44100 Ferrara, Italy

Received 20 December 2007; received in revised form 19 March 2008; accepted 31 March 2008
Handling Editor M.P. Cartmell
Available online 9 June 2008

Abstract

In the last decades, various methods have been proposed for the experimental evaluation of tensile forces acting in tie-beams of arches and vaults. Moreover, static and dynamic approaches have been formulated to evaluate critical compressive axial forces and flexural stiffness of end constraints. Adopting Euler–Bernoulli beam model, this paper shows that, if bending stiffness and mass per unit length of a beam with constant cross-section are known, the axial force and the flexural stiffness of the end constraints can be deduced by one vibration frequency and three components of the corresponding mode shape. Finally, data conditions are given to assess a physically admissible identification of the unknown parameters.

1. Introduction

Many engineering applications concern the axial load identification of uniform simply supported beams in the presence of end rotational elastic constraints. For instance, experimental techniques have more or less recently been proposed to evaluate tensile forces acting in tie-beams of arches or vaults [1–7] as well as critical compressive forces of beams with unknown end rotational conditions [8–16]. Usually, geometric beam properties can be directly evaluated with reasonable accuracy whereas the constraint flexural stiffness or the axial force cannot easily be obtained by direct measurements. Finite element (FE) formulations coupled with model updating techniques were proposed for beams and frameworks in the presence of both translational and rotational elastic supports [17–20]. However, in these formulations, nonuniqueness of estimated parameters may arise.

In particular, for the evaluation of tensile forces acting in tie-beams, static and dynamic methods have been proposed. Static methods make use of displacements and deformations of tie-beams subjected to one or more concentrated loads. For instance, in Refs. [1,2] a static force is applied at mid-span and displacements, as well as axial deformations at the two opposite sides of the cross-section, are evaluated at three selected locations

*Corresponding author. Tel.: +390532974886; fax: +390532974870.
E-mail addresses: nerio.tullini@unife.it (N. Tullini), ferdinando.laudiero@unife.it (F. Laudiero).

0022-460X/$ - see front matter © 2008 Elsevier Ltd. All rights reserved.
doi:10.1016/j.jsv.2008.03.061

giving rise to nine distinct measurements; hence, a unique solution for the tensile force and the bending moments at the end sections is obtained.

In dynamic methods, vice versa, resort is made to vibration tests making use of beam model parameters. In Refs. [3,4], an approximate method is proposed, using both static deflections and vibration frequencies to evaluate axial forces in tie-beams. Making use of the first three modal frequencies, a numerical method was suggested [6], which is based on a minimization procedure of a proper error function; hence, the tensile force and the beam bending stiffness are obtained. Making use of a FE model, a weighted least-squares estimation method is presented in Ref. [17], which alternatively uses the two or three lowest frequencies, or the two lowest frequencies with their corresponding (normalized) mode shapes. Moreover, to determine both plane- and space-frame forces, sensitivity-based methods are used in Refs. [7,18,19].

The experimental evaluation of critical compressive forces of beams with unknown boundary conditions was widely investigated as well. In the static approach proposed by Southwell [8,9], the deflection f at mid-span is measured for different values of the compressive force N and the critical value is extrapolated by means of a proper plot reporting f versus f/N ratio. In Ref. [10], reduction of natural frequencies as the value of the compressive force increases is adopted as the ruling parameter and the critical axial load is estimated by assuming a linear relation between the axial load and the square of natural frequencies (see Eq. (9) reported in the following). As a matter of fact, approximate formulas of this type need an *a-priori* estimate of the end constraint stiffness and are quite accurate for known boundary conditions only [11,12,21]. In Refs. [13,14], the vibration mode shapes are used to give a kernel approximation for the integral formulation of the (column) elastic stability problem. In Ref. [15], the vibration mode shapes are used to formulate a FE model for the critical load estimation. In Refs. [13–15], knowledge of end constraint stiffness is not required; vice versa, in Refs. [16,22,23] stiffness of end constraints of a prismatic column subjected to null axial load are determined first and, then, the critical load is analytically derived.

The identification method proposed hereafter is based on the Euler–Bernoulli beam model and assumes geometric and elastic properties as known parameters. Making use of any natural frequency and of three displacement components of the corresponding mode shape, it is shown that both axial loads and stiffness of end flexural springs of a beam subjected to tensile or compression forces can easily be obtained. Moreover, relations between mode shape displacements and axial resultants are determined, so as to assess proper data conditions for a physically correct identification of the unknown parameters. As for compression resultants, the proposed method offers both forces acting in slender beams and flexural constraint stiffness; hence, critical loads can analytically be evaluated and compared with actual compression forces, giving an experimental evaluation of the safety factor.

Validation of this technique was obtained by laboratory and *in-situ* tests, including comparisons [5] with magnetostriction technique (Barkhausen method). In particular, the proposed method was repeatedly applied in the consolidation design of vault arcades of monumental buildings where fractured tie-rods were in need of substitution.

2. Governing equations

The problem of a prismatic single-span beam subjected to a constant axial load, with end elastic rotational constraints, has been the subject of a massive study in the past years [24,25]. A comprehensive summary of this work is given in Refs. [21,26–28]. The reference model is constituted by a simply supported prismatic beam of length L, constrained by two end elastic-springs with k_0 and k_1 flexural stiffness, subjected to an axial resultant N (positive sign is assigned to tensile forces). Young's modulus E, mass per unit length μ and cross-section second area moment J are assumed to be constant, and known as well (Fig. 1).

Making use of the nondimensional coordinate $x = X/L$ and neglecting both rotatory inertia and shear deformations, circular frequencies ω and vibration modes $v(x)$ are ruled by the following eigenvalue problem [25–28]:

$$v''''(x) - nv''(x) + \lambda^4 v(x) = 0, \quad \text{in } 0 < x < 1, \tag{1}$$

$$v(0) = 0, \quad v''(0) - \beta_0 v'(0) = 0, \quad \text{for } x = 0, \tag{2a,b}$$

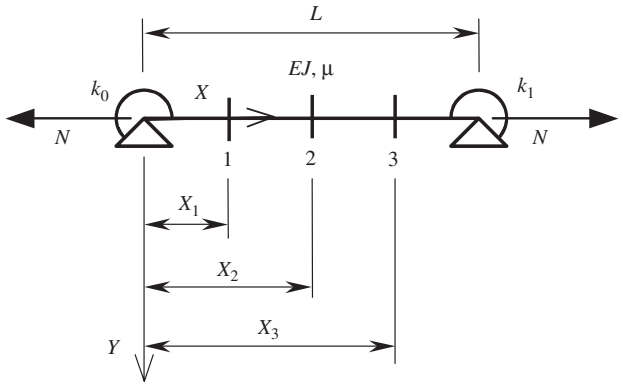

Fig. 1. Beam with end flexural constraints and location of the instrumented sections.

$$v(1) = 0, \quad v''(1) + \beta_1 v'(1) = 0, \ \text{for} \ x = 1, \tag{3a,b}$$

where prime means derivation with respect to x and

$$n = \frac{NL^2}{EJ}, \quad \lambda^4 = \omega^2 \frac{\mu L^4}{EJ}, \quad \beta_0 = \frac{k_0 L}{EJ}, \quad \beta_1 = \frac{k_1 L}{EJ}. \tag{4a,b,c,d}$$

Hence, solution to Eq. (1) takes the form

$$v(x) = C_1 \cos q_1 x + C_2 \sin q_1 x + C_3 \cosh q_2 x + C_4 \sinh q_2 x, \tag{5}$$

where

$$q_1^2 = \tfrac{1}{2}\left(\sqrt{n^2 + 4\lambda^4} - n\right), \quad q_2^2 = \tfrac{1}{2}\left(\sqrt{n^2 + 4\lambda^4} + n\right) = q_1^2 + n. \tag{6a,b}$$

Boundary conditions (2,3) and frequency characteristic equation (see Eq. (20) reported in the following) furnish integration constants C_1–C_4 and q_1, respectively. Eqs. (6) yield $\lambda^2 = q_1 q_2$ and in particular, when the axial resultant n vanishes, $\lambda = q_1 = q_2$ is readily obtained. Making use of Eqs. (4a,b) and (6b), any given beam circular frequency ω can be written in the form:

$$\omega = 2\pi f = \lambda^2 \sqrt{\frac{EJ}{\mu L^4}} = q_1 q_2 \sqrt{\frac{EJ}{\mu L^4}} = q_1^2 \sqrt{\frac{EJ}{\mu L^4}} \sqrt{1 + \frac{n}{q_1^2}} = q_1 \sqrt{\frac{N}{\mu L^2}} \sqrt{1 + \frac{q_1^2}{n}}. \tag{7}$$

Considering the first vibration frequency, Fig. 2 shows the plot q_1 versus $1/\sqrt{n}$ for a beam subjected to tensile forces and symmetric boundary conditions with $\beta_0 = \beta_1 = \beta = 0$, 2, 10, 20, 50, respectively.

When the end constraint stiffness β goes to zero, coefficient q_1 tends to π and is no longer dependent on n. Hence, Eq. (7) becomes

$$\omega_1 = \pi^2 \sqrt{\frac{EJ}{\mu L^4}} \sqrt{1 + \frac{N}{N_{\mathrm{cr}\,E}}}, \tag{8}$$

where $N_{\mathrm{cr}\,E} = \pi^2 EJ/L^2$ represents the first Eulerian critical load. Coefficient q_1 approaches π (for any β) when $1/\sqrt{n}$ becomes small. In other words, if the tensile force is very high, frequencies do not depend on boundary conditions anymore and the beam behaves as if it were a taut string. Hence, substituting the first (experimental) vibration frequency ω_1 into Eq. (8) yields the unknown axial force

$$N = N_{\mathrm{cr}\,E}\left(\frac{\omega_1^2}{\pi^4}\frac{\mu L^4}{EJ} - 1\right) = N_{\mathrm{cr}\,E}\left[\left(\frac{\lambda_1}{\pi}\right)^4 - 1\right]. \tag{9}$$

For a beam fully clamped at both ends ($\beta_0 = \beta_1 = \beta = \infty$), when the axial force vanishes ($n = 0$), coefficient q_1 attains a limit value for the first vibration frequency, i.e., $q_1 = 1.506 * \pi = 4.730$. Moreover, for $1/\sqrt{n}$ sufficiently small, Rayleigh [24] obtained the simple expression $q_1 = \pi\left(1 + 2/\sqrt{n}\right)$ (Fig. 2), which can be

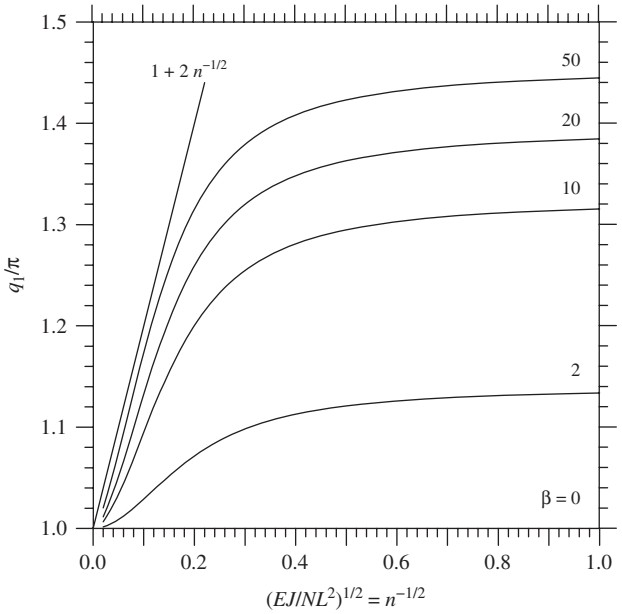

Fig. 2. First vibration frequency: plot of q_1 versus $1/\sqrt{n}$ for different values of flexural stiffness β of end constraints.

substituted in Eq. (7) to obtain a first order approximation of ω_1. A slightly more accurate approximation is reported in Ref. [29]:

$$\omega_{1,\text{clamped}} \cong \omega_{1,\text{string}}\left[1+\frac{2}{\sqrt{n}}+\left(4+\frac{\pi^2}{2}\right)\frac{1}{n}\right], \tag{10}$$

where $\omega_{1,\text{string}} = \pi\sqrt{N/\mu L^2}$ is the first circular vibration frequency of a taut string. The error between $\omega_{1,\text{clamped}}$ and $\omega_{1,\text{string}}$ is less than 1% if $1/\sqrt{n} < 0.005$. This value has been assumed in test guidelines [30] for cable force determination to asses the range of validity of string theory. In fact, dynamic behavior of a stay cable is between the limit cases of a taut string and of a stiff cable with fixed ends [31].

3. Identification of stiffness constraints and axial forces

In order to identify the axial load N and the stiffness k_0 and k_1 of the end flexural constraints, knowledge is required of one vibration frequency and the corresponding mode shape at three locations of coordinates X_1, X_2 and X_3 (Fig. 1). With reference to the nondimensional coordinate $x = X/L$, three displacements are assumed to have been determined and denoted by $v_i = v(x_i)$ for $i = 1, 2, 3$. Hence, constants $C_1,\ldots,C_4$ can be determined to the accuracy of a constant and the mode shape (5) is finally obtained. In fact, substituting Eq. (5) into boundary condition (2a) yields $C_3 = -C_1$ and the same Eq. (5) reduces to

$$v(x) = C_1(\cos\, q_1 x - \cosh\, q_2 x) + C_2\, \sin\, q_1 x + C_4\, \sinh\, q_2 x. \tag{11}$$

Hence, the following linear equation system is obtained:

$$\begin{bmatrix} \cos\, q_1x_1 - \cosh\, q_2x_1 & \sin\, q_1x_1 & \sinh\, q_2x_1 \\ \cos\, q_1x_2 - \cosh\, q_2x_2 & \sin\, q_1x_2 & \sinh\, q_2x_2 \\ \cos\, q_1x_3 - \cosh\, q_2x_3 & \sin\, q_1x_3 & \sinh\, q_2x_3 \end{bmatrix} \begin{Bmatrix} C_1 \\ C_2 \\ C_4 \end{Bmatrix} = \begin{Bmatrix} v_1 \\ v_2 \\ v_3 \end{Bmatrix} \tag{12}$$

Coefficients C_1, C_2 and C_4 are linear functions of the three (experimental) amplitudes v_1, v_2, v_3, and depend on the unknown parameter n and on constant λ through coefficients q_1 and q_2 reported in Eqs. (6). In its turn, λ depends on the experimental circular frequency ω. By imposing the boundary condition (3a), the following

transcendental equation is obtained, to be solved for the unknown constant n:

$$C_1(n,\lambda)(\cos\ q_1(\lambda,n) - \cosh\ q_2(\lambda,n)) + C_2(\lambda,n)\sin\ q_1 + C_4(\lambda,n)\sinh\ q_2(\lambda,n) = 0. \tag{13}$$

Finally, relations (2b, 3b) yield coefficients β_0 and β_1:

$$\beta_0 = \frac{v''(0)}{v'(0)} = -\frac{(q_1^2+q_2^2)C_1}{C_2 q_1 + C_4 q_2}, \tag{14}$$

$$\beta_1 = -\frac{v''(1)}{v'(1)} = \frac{(q_1^2+q_2^2)(C_1\cos\ q_1 + C_2\sin\ q_1)}{-C_1(q_1\sin\ q_1 + q_2\sinh\ q_2) + C_2\, q_1\cos\ q_1 + C_4\, q_2\cosh\ q_2}. \tag{15}$$

It should be noted that v_1, v_2, and v_3 are admissible if positive values of nondimensional stiffness coefficients β_0 and β_1 are consequently derived.

4. Control points located at the middle and at $\frac{1}{4}$ and $\frac{3}{4}$ of the beam span

The above formulation can be simplified if control points are assumed at sections having nondimensional coordinates $x_1 = 1/4$, $x_2 = 1/2$, and $x_3 = 3/4$. In this case, if the mid-section does not coincide with a node of the assumed mode shape, i.e., if $v_2 \neq 0$, Eqs. (13)–(15), respectively, yield

$$\frac{v_1+v_3}{v_2} = \frac{1+2\cos(q_1/4)\cosh(q_2/4)}{\cos(q_1/4)+\cosh(q_2/4)}, \tag{16}$$

$$\beta_0 = (q_1^2+q_2^2)\frac{a(v_1/v_2)-b}{c(v_1/v_2)-d}, \quad \beta_1 = (q_1^2+q_2^2)\frac{a(v_3/v_2)-b}{c(v_3/v_2)-d}, \tag{17a,b}$$

where constants a, b, c, d are given by the following relations:

$$a = \sin\ q_1\ \sinh\frac{q_2}{2} - \sin\frac{q_1}{2}\sinh\ q_2, \quad b = \sin\ q_1\ \sinh\frac{q_2}{4} - \sin\frac{q_1}{4}\sinh\ q_2, \tag{18a,b}$$

$$c = 2\left(\cos\frac{q_1}{2} - \cosh\frac{q_2}{2}\right)\left(q_1\ \cos\frac{q_1}{2}\sinh\frac{q_2}{2} - q_2\ \sin\frac{q_1}{2}\cosh\frac{q_2}{2}\right), \tag{18c}$$

$$\begin{aligned} d = {} & q_1\left(\cos\ q_1\ \sinh\frac{q_2}{4} + \sinh\frac{3q_2}{4} - \cos\frac{q_1}{4}\sinh\ q_2\right) \\ & + q_2\left(\cosh\ q_2\sin\frac{q_1}{4} + \sin\frac{3q_1}{4} - \cosh\frac{q_2}{4}\sin\ q_1\right). \end{aligned} \tag{18d}$$

The transcendental equation (16) provides for values of n corresponding to any (experimental) value of λ. Moreover, if the first mode shape gives $v_1 = v_3$ or the second mode shape shows $v_2 = 0$, then symmetric boundary conditions are ascertained.

4.1. Particular cases of end constraint stiffness

Rearranging Eqs. (17), alternative relations for mode shape amplitudes ratios can be obtained:

$$\frac{v_1}{v_2} = \frac{(q_1^2+q_2^2)b - d\beta_0}{(q_1^2+q_2^2)a - c\beta_0}, \quad \frac{v_3}{v_2} = \frac{(q_1^2+q_2^2)b - d\beta_1}{(q_1^2+q_2^2)a - c\beta_1}. \tag{19a,b}$$

Equating the sum of Eqs. (19) to the right-hand side of Eq. (16) and making use of Eqs. (18) yield the frequency characteristic equation [26,27], in the form

$$\begin{aligned} & (q_1^2+q_2^2)^2\sin\ q_1\ \sinh\ q_2 + (\beta_0+\beta_1)(q_1^2+q_2^2)(q_2\sin\ q_1\cosh\ q_2 - q_1\cos\ q_1\sinh\ q_2) \\ & + \quad \beta_0\beta_1\left[2q_1q_2(1-\cos\ q_1\cosh\ q_2) + (q_2^2-q_1^2)\sin\ q_1\sinh\ q_2\right] = 0. \end{aligned} \tag{20}$$

In particular, for beams having one pinned end only, e.g., $\beta_0 = 0$, Eqs. (19) yield

$$\frac{v_1 + v_3}{v_2} = \frac{b}{a} + \frac{(q_1^2 + q_2^2)b - d\beta_1}{(q_1^2 + q_2^2)a - c\beta_1}. \tag{21}$$

For simple supported beams ($\beta_0 = \beta_1 = 0$), Eq. (20) yields the classical result as follows:

$$\sin q_1 = 2 \cos\frac{q_1}{2}\sin\frac{q_1}{2} = 0 \Rightarrow q_1 = m\pi, \quad q_2 = \frac{\lambda^2}{m\pi} \quad \text{for } m = 1, \ldots, \infty. \tag{22a,b}$$

Moreover, using Eqs. (18a,b) and coefficients q_1, q_2 reported in Eqs. (22b), Eq. (21) can be written in the form

$$\frac{v_1 + v_3}{2v_2} = \frac{b}{a} \Rightarrow \frac{v_1 + v_3}{2v_2} = \frac{1}{2\cos(m\pi/4)} \quad \text{for } m \text{ odd}. \tag{23a,b}$$

Hence, $(v_1 + v_3)/(2v_2) = 1/\sqrt{2}$ for $m = 1, 7, 9, 15, 17$, etc. and $(v_1 + v_3)/(2v_2) = -1/\sqrt{2}$ for $m = 3, 5, 11, 13$, etc. Moreover, referring to even eigenvalues λ and making use of coefficients q_1, q_2 reported in Eqs. (22b), the constant a given in Eq. (18a) vanishes, the beam mid-section coincides with a node (i.e., $v_2 = 0$) and mode shape amplitude ratio (23) cannot be defined. Nevertheless, for boundary conditions $\beta_0 = 0$ and β_1 very small, Eqs. (22) still hold: that is to say that coefficients q_1, q_2 of such "nearly pinned" beam coincide with the analogous values of a simply supported beam. Substituting coefficients q_1, q_2 reported in Eqs. (22b) into Eq. (16) yields

$$\frac{v_1 + v_3}{v_2} = \frac{1 + 2\cos(m\pi/4)\cosh(\lambda^2/4m\pi)}{\cos(m\pi/4) + \cosh(\lambda^2/4m\pi)} \quad \text{for } m \text{ even}. \tag{24}$$

In pinned–clamped beams, e.g., $\beta_0 = 0$ and $\beta_1 = \infty$, Eq. (20) yields the classical result:

$$q_2 \sin q_1 \cosh q_2 - q_1 \cos q_1 \sinh q_2 = 0 \tag{25}$$

and, consequently, Eq. (21) becomes

$$\frac{v_1 + v_3}{v_2} = \frac{b}{a} + \frac{d}{c}. \tag{26}$$

Analogously, in clamped–clamped beams ($\beta_0 = \beta_1 = \infty$), Eqs. (20) and (21) yield

$$2q_1q_2(1 - \cos q_1 \cosh q_2) + (q_2^2 - q_1^2)\sin q_1 \sinh q_2 \tag{27a}$$

$$= \left(q_1 \cos\frac{q_1}{2}\sinh\frac{q_2}{2} - q_2 \sin\frac{q_1}{2}\cosh\frac{q_2}{2}\right)\left(q_1 \sin\frac{q_1}{2}\cosh\frac{q_2}{2} + q_2 \cos\frac{q_1}{2}\sinh\frac{q_2}{2}\right) = 0, \tag{27b}$$

$$\frac{v_1 + v_3}{2v_2} = \frac{d}{c} \quad \text{for odd eigenvalues } \lambda. \tag{28}$$

For even eigenvalues λ, the constant c given by Eq. (18c) is equal to zero.

4.2. Admissible data

From a mathematical point of view, inverse vibration problems require necessary and sufficient conditions to be satisfied by the spectral data to ensure that a feasible solution is obtained. In fact, two kinds of improper assumptions can be made. First of all, improper values for mass distribution μ, elastic modulus E, and cross-section second area moment could be adopted. In addition to this, the experimental data are worked out by means of a mechanical model: i.e., the Euler–Bernoulli beam model. If the beam were not slender enough, inadmissible final results could be drawn.

For the problem at hand, to obtain positive values [32] for stiffness coefficients β_0 and β_1, both numerators and denominators in Eqs. (17) must have positive or negative sign. In the following, by example, the first case is reported only.

$$\beta_0, \beta_1 \geqslant 0 \;\Rightarrow\; \begin{cases} a\dfrac{v_1}{v_2} - b \geqslant 0 \\ c\dfrac{v_1}{v_2} - d \geqslant 0 \end{cases} \quad \text{and} \quad \begin{cases} a\dfrac{v_3}{v_2} - b \geqslant 0, \\ c\dfrac{v_3}{v_2} - d \geqslant 0. \end{cases} \tag{29a,b}$$

Eqs. (29) together with Eqs. (16) and (18) imply

$$\begin{cases} a\left(\dfrac{v_1 + v_3}{2v_2}\right) - b \geqslant 0 \\ c\left(\dfrac{v_1 + v_3}{2v_2}\right) - d \geqslant 0 \end{cases} \Rightarrow \begin{cases} \left(\cos\dfrac{q_1}{2}\right)\sin\dfrac{q_1}{4} \leqslant 0 \\ \left(q_1 \sin\dfrac{q_1}{2}\cosh\dfrac{q_2}{2} + q_2 \cos\dfrac{q_1}{2}\sinh\dfrac{q_2}{2}\right)\sin\dfrac{q_1}{4} \geqslant 0 \end{cases} \tag{30a,b}$$

The two inequalities (30a) provide for admissible data areas reported in Fig. 3. For odd eigenvalues λ, admissible couples (n, λ) are delimited by curves corresponding to the limit cases of simply supported and fully clamped beams. In fact, reducing Eqs. (30a) to two equalities, they coincide with Eqs. (23a) and (28) corresponding to pinned–pinned and clamped–clamped beams, respectively. Likewise, when bracketed factors in Eqs. (30b) are set equal to zero, frequency characteristic equation (22a) is re-obtained and Eq. (27b) turns out to be satisfied.

With reference to even eigenvalues λ, it worth noting that inequalities (29b) give rise to pinned–clamped beam equation (26). In fact, reducing Eqs. (30a) to two equalities and summing their left-hand sides, Eq. (26) is re-obtained. Furthermore, Eq. (24) holding for "nearly pinned" beams can be adopted as an additional curve to define admissible data areas in $n-\lambda$ plot (Fig. 3). Hence, admissible couples (n, λ) are also delimited by curves corresponding to the limit cases of pinned–clamped beams and "nearly pinned" beams.

Fig. 3 shows the plot of ratio $(v_1 + v_3)/(2v_2)$ versus λ for both positive and negative values of n. In particular, dotted lines represent the graph of Eq. (16) for $n = -4\pi^2$, $-\pi^2$, 0, 10, 100, 1000, 10000. Moreover, thin solid lines follow from Eqs. (23) and (28) and Eqs. (24) and (26), for odd and even eigenvalues λ, respectively. Also, Fig. 3 reproduces admissible data areas corresponding to the first nine eigenvalues and thick solid lines represent couples satisfying inequalities (29a) for some particular values of n. For simply supported beams, $(\beta_0 = \beta_1 = 0)$, the eigenfunctions coincide with the Eulerian critical shapes:

$$v(x) = C \sin m\pi x, \quad m = 1, \ldots, \infty. \tag{31}$$

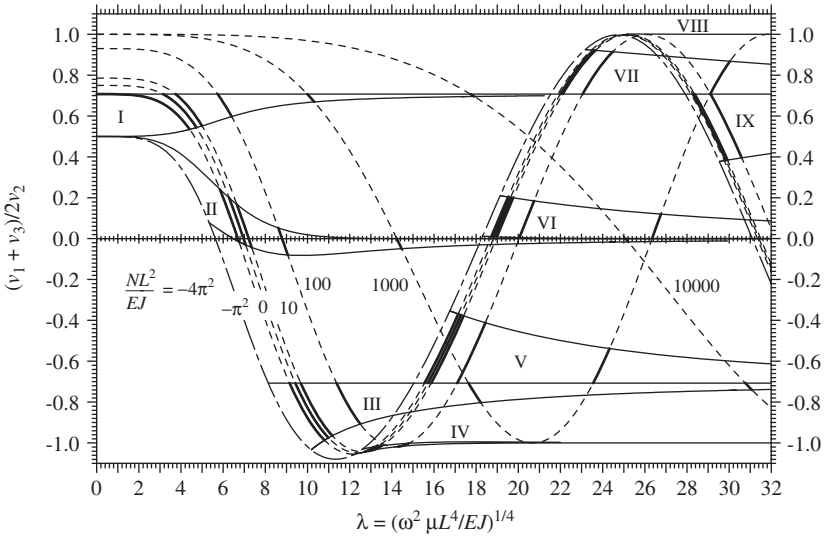

Fig. 3. Ratio $(v_1 + v_3)/2v_2$ versus λ for the first nine frequencies, for some given values of n.

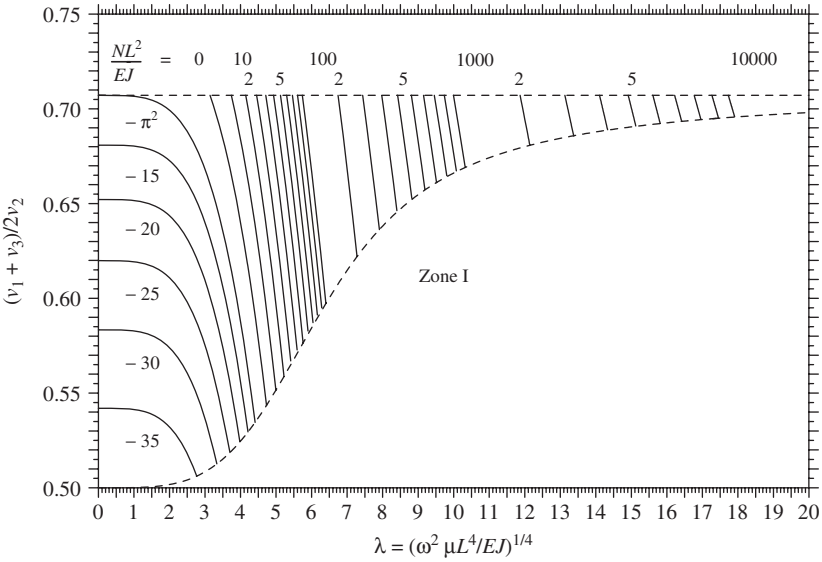

Fig. 4. Ratio $(v_1+v_3)/2v_2$ versus λ for the first vibration frequency, for some given values of n.

In this case, Eq. (23b) holds for any given value of n and the first vibration frequency vanishes for $n=-\pi^2$ corresponding to the first Eulerian critical load. Moreover, it is to be noted that the minimum value for n corresponds to the first critical load of a fully clamped beam ($\beta_0=\beta_1=\infty$) having nondimensional value $n=-4\pi^2$ and mode shape:

$$v(x)=C(1-\cos 2\pi x). \tag{32}$$

In fact, Eq. (32) yields $(v_1+v_3)/2v_2=0.5$ and, consequently, the first vibration frequency vanishes for the couple $[n,\ (v_1+v_3)/2v_2]=[-4\pi^2,\ 0.5]$.

Fig. 4 magnifies the area no. I of Fig. 3, reproducing Eq. (16) for some particular values of the nondimensional axial force n. Therefore, Fig. 4 represents a plot where the point of experimental coordinates $[(v_1+v_3)/2v_2,\ \lambda]$ can be located; hence, the curve NL^2/EJ containing the experimental point yields the unknown value of the axial force N.

It can be observed that, for $n>10000$, i.e., for $1/\sqrt{n}<0.01$, the dotted lines corresponding to the limit cases of simply supported and fully clamped beams, tend to coincide. Hence, it is confirmed that, for high values of N, the evaluation of tensile forces does not depend on the boundary conditions and Eq. (9) can usefully be employed.

5. Laboratory tests

In civil or mechanical engineering, when a single span of a continuous beam is to be analyzed, the adjacent beams behave as elastic constraints with respect to the beam under investigation. Therefore, it is usual to idealize the adjacent beams as rotational springs and the beam under investigation as if it were constrained by elastic rotational springs at one or both ends. This is the reason why a reference model of a beam resting on rigid supports and constrained by two end rotational springs is commonly adopted. In the laboratory tests reported in the following, the end rotational springs were brought back to adjacent spans of a continuous beam and the stiffness values of the rotational springs were assumed to coincide with the flexural stiffness of the adjacent beams. In the case of a vault tie-rod restrained by lateral masonry walls, the masonry behavior at the rod ends is modelled again with elastic rotational springs which reproduce the restraining effect of the masonry walls. In fact, as far as vibrations imply very small deflections, a purely elastic model can be acceptable.

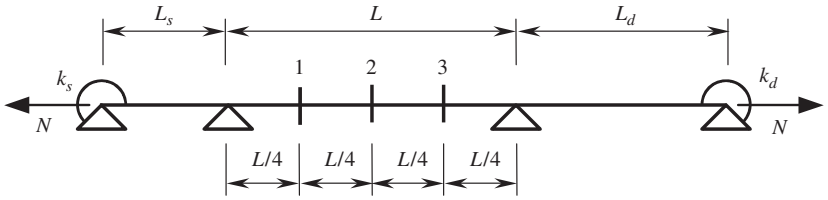

Fig. 5. Beam experimental model for tensile and compression tests.

For the laboratory tests, tie-rods or slender box beams were adopted. At one end, an hydraulic jack was adopted to assign the axial force and, at the other end, a 100 kN load cell was placed, with accuracy of 2 mV/V. For tensile tests, a rod with 20 mm diameter was adopted and Young's modulus $E = 196$ GPa and density $\rho = 7850\,\mathrm{kg/m^3}$ were experimentally evaluated. For compression tests, a slender box beam with section $80 \times 30 \times 3\,\mathrm{mm^3}$ was adopted and Young's modulus $E = 206$ GPa and density $\rho = 7850\,\mathrm{kg/m^3}$ were analogously obtained. Two additional supports were introduced at intermediate section so as to have two outer spans simulating end constraints of variable stiffness (Fig. 5). As for the end springs, the analytical investigation considered the limit cases ($k_s = k_d = 0$) and ($k_s = k_d = \infty$) only because of the difficulty of evaluating the rotational stiffness introduced by the experimental equipment.

For the limit cases considered, the stiffness coefficients β_0 and β_1 of the central beam take the values [8,33]:

$$\beta_0 = \frac{3L}{L_s}\frac{1}{I_1(\alpha_s)} \quad \text{for } k_s = 0, \quad \beta_0 = \frac{4L}{L_s}\frac{3I_1(\alpha_s)}{4I_1^2(\alpha_s) - I_2^2(\alpha_s)} \quad \text{for } k_s = \infty, \tag{33a,b}$$

$$\beta_1 = \frac{3L}{L_d}\frac{1}{I_1(\alpha_d)} \quad \text{for } k_d = 0, \quad \beta_1 = \frac{4L}{L_d}\frac{3I_1(\alpha_d)}{4I_1^2(\alpha_d) - I_2^2(\alpha_d)} \quad \text{for } k_d = \infty, \tag{34a,b}$$

where $\alpha_s = L_s/L\sqrt{n}$, $\alpha_d = L_d/L\sqrt{n}$, and

$$I_1(\alpha) = \frac{3}{\alpha}\left(\frac{1}{\tanh\,\alpha} - \frac{1}{\alpha}\right), \quad I_2(\alpha) = \frac{6}{\alpha}\left(\frac{1}{\alpha} - \frac{1}{\sinh\,\alpha}\right) \quad \text{for } \alpha = \alpha_s, \alpha_d. \tag{35a,b}$$

When the axial resultant N vanishes, i.e., $n = 0$, coefficients α_s, α_d are equal to zero and Eqs. (35) reduce to $I_1(0) = I_2(0) = 1$. Consequently, Eqs. (33) and (34) yield the stiffness coefficients [33] for simply supported ($k_s = k_d = 0$) and hinged–clamped ($k_s = k_d = \infty$) beams, respectively:

$$k_0 = \frac{3EJ}{L_s}, \quad k_1 = \frac{3EJ}{L_d} \quad \text{for } k_s = k_d = 0, \quad k_0 = \frac{4EJ}{L_s}, \quad k_1 = \frac{4EJ}{L_d} \quad \text{for } k_s = k_d = \infty. \tag{36a,b,c,d}$$

Three piezoelectric accelerometers PCB/353B18, having sensitivity of 10 mV/g and weight of 1.8 g, were fastened in the central span, at equal distances, by means of metallic wrappers. Dynamic tests were performed, hitting the instrumented sections with an impact hammer PCB/086C04, able to measure a pulse up to 4.4 kN with sensitivity of 1.2 mV/N. All the instruments were connected to a signal conditioner and, finally, to a PC data acquisition system. Tests were performed hitting, three times, each of the three instrumented sections of the central span. Fig. 6 shows an example of the time histories and the frequency spectra of the impact hammer and of three accelerometers for a given pulse. As is known [34,35], the ratio between the Fast Fourier Transform (FFT) of the acceleration $a_i(t)$ and the FFT of the pulse $F_j(t)$ yields the inertance Frequency Response Function (FRF) H_{ij}. Hence, the inertance FRF H_{ij} at section x_i for an impulse load at section x_j [25], is given by

$$H_{ij}(\omega) = -\frac{\omega^2}{\mu L}\sum_{r=1}^{\infty}\frac{v_i^{(r)}v_j^{(r)}\Big/\left\|v^{(r)}\right\|^2}{\omega_r^2 - \omega^2 + 2\mathrm{i}\zeta_r\omega_r\omega}, \tag{37}$$

where ω_r, ζ_r, $v^{(r)}$ are the circular natural frequency, the damping ratio defined by $c/(2\mu\omega_r)$ and the rth mode shape, respectively and, finally, $\left\|v^{(r)}\right\|^2 = \int_0^1 \left(v^{(r)}\right)^2 \mathrm{d}x$. For a low damping ratio, when the vibration

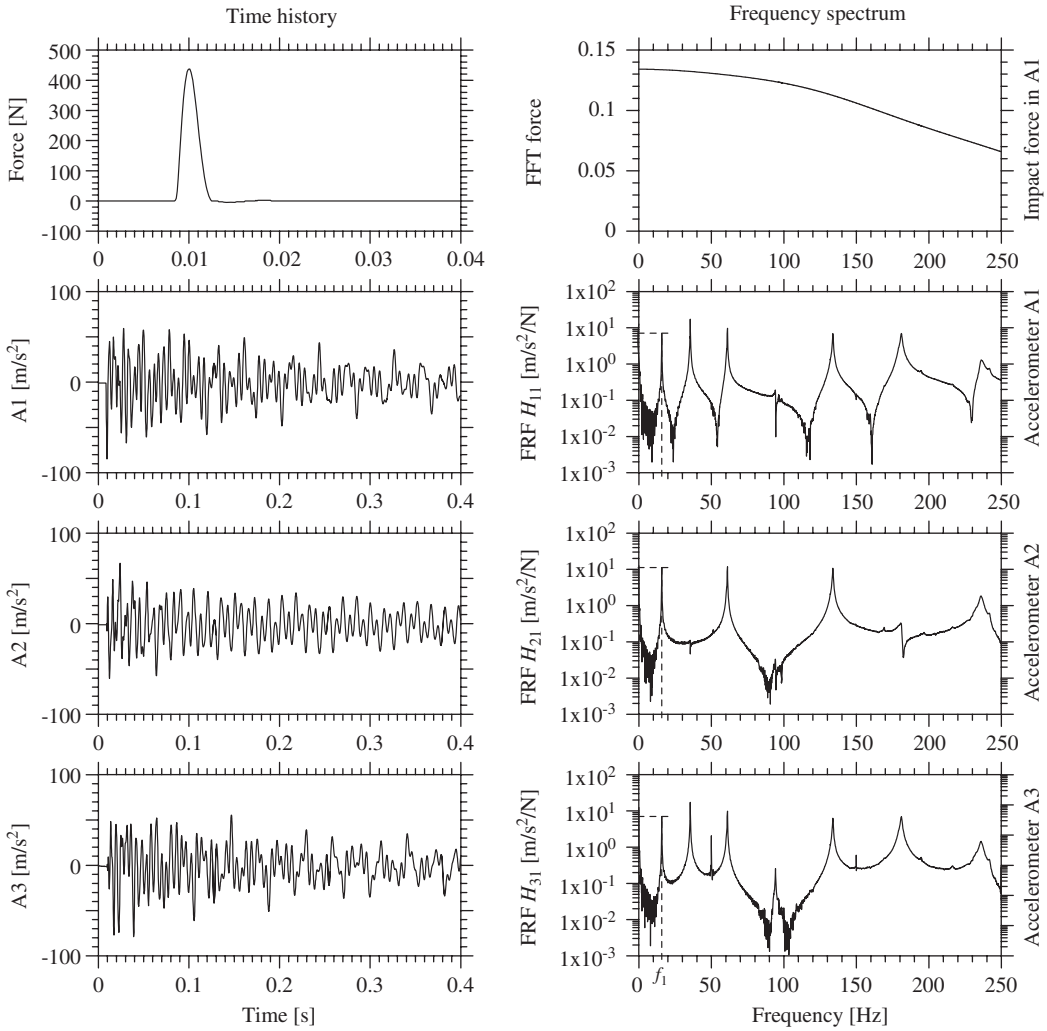

Fig. 6. Time history and frequency spectrum for the impact hammer and three instrumented sections.

frequencies are not very close to each other, in the neighborhood of a given circular frequency ω_s, Eq. (37) admits the following approximation:

$$H_{ij}(\omega) \cong -\frac{\omega^2}{\mu L}\frac{v_i^{(s)}v_j^{(s)}\Big/\left\|v^{(s)}\right\|^2}{\omega_s^2-\omega^2+2\mathrm{i}\zeta_s\omega_s\omega} \quad \text{for } \omega \cong \omega_s. \tag{38}$$

Then, the contributions of modes with different circular frequencies can be neglected, and the frequency domain analysis of the vibrating beam reduces to that of an independent simple oscillator. Consequently, the peak-picking method [34,35] can usefully be adopted. In other words, natural frequencies are located at each peak of the inertance moduli (Fig. 6) and the damping value can be estimated with the half-power method [34]. As a matter of fact, for the first three frequencies of the beam investigated, damping ratios turned out to be less than 5% (Fig. 6) so as to justify the use of Eq. (38). Finally, Eq. (38) shows that the (sth) eigenvalue components are proportional to the inertance modulus peaks. Then, hitting the jth instrumented section, the following ratios are obtained:

$$\frac{v_1^{(s)}}{v_2^{(s)}}=\frac{\left|H_{1j}(\omega_s)\right|}{\left|H_{2j}(\omega_s)\right|}, \quad \frac{v_s^{(s)}}{v_2^{(s)}}=\frac{\left|H_{3j}(\omega_s)\right|}{\left|H_{2j}(\omega_s)\right|}. \tag{39}$$

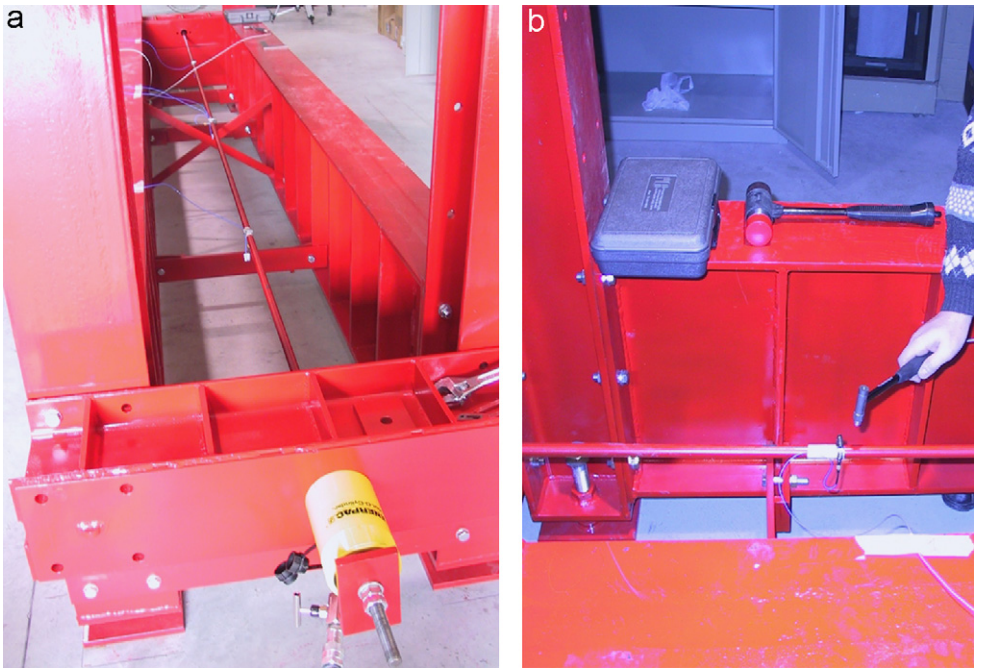

Fig. 7. Experimental tensile test rig. The rod is pulled by the hydraulic jack (a). The hammer hits the rod in the proximity of an instrumented section (b).

Table 1
Tensile vibration tests. Average of the experimental parameters

Test	N_x (kN)	f_1 (Hz)	v_1/v_2	v_3/v_2
1	1.45	6.66	0.624	0.611
2	2.97	7.63	0.626	0.621
3	4.95	8.70	0.633	0.622
4	10.22	10.91	0.647	0.631
5	30.15	16.76	0.668	0.659
6	50.00	20.98	0.680	0.663

Table 2
Tensile vibration tests. Experimental and estimated parameters

Test	Experimental data		Estimated parameters			
	λ	$(v_1+v_3)/2v_2$	n_a	N_a (kN)	β_0	β_1
1	4.69	0.618	15.09	1.64	13.4	12.9
2	5.02	0.624	28.98	3.25	14.7	12.9
3	5.36	0.628	45.84	5.20	16.0	15.0
4	6.01	0.639	89.78	10.28	17.7	17.7
5	7.44	0.663	259.88	29.89	23.2	18.8
6	8.33	0.671	427.15	49.16	26.1	25.7

Alternative identification techniques determine the modal parameters by means of output-only measurements, deriving from unknown inputs. In this context, knowledge of the excitation is usually replaced by the assumption that the system is excited by white Gaussian noise [35]. For instance, the

stochastic-subspace-identification technique makes it possible to determine closely spaced frequencies, corresponding to in-plane and out-of-plane mode shapes. This method is applied for testing stay cables using ambient vibration measurements [31].

5.1. Tensile tests

As for tensile tests (Fig. 5), the case $L_s = 797\,\text{mm}$, $L = 3625\,\text{mm}$, and $L_d = 985\,\text{mm}$ is reported in the following. Fig. 7 shows the rod subjected to the vibration test. Tables 1 and 2 show measured and estimated mean parameters, respectively. Fig. 8a shows excellent agreement between measured and estimated loads N_x and N_a. In particular, the nine experimental values of the tensile forces are very close to each other for each of the assigned forces N_x, giving a highly reliable average value for N_a (Fig. 8a).

Fig. 9 shows the (estimated) variation of the end constraint stiffness β_0 and β_1 versus the tensile force N. Dotted lines correspond to the limit values given by Eqs. (33) and (34). Cross-symbols correspond to single test evaluations and solid lines represent the average of the nine experimental data. It can be noted that, at the beam end in front of the load cell, the estimate of the elastic parameter (β_0) is quite reasonable. Vice versa, at the opposite end in front of the hydraulic jack, β_1 estimation is not satisfactory at all. Yet, if β_1 is calculated

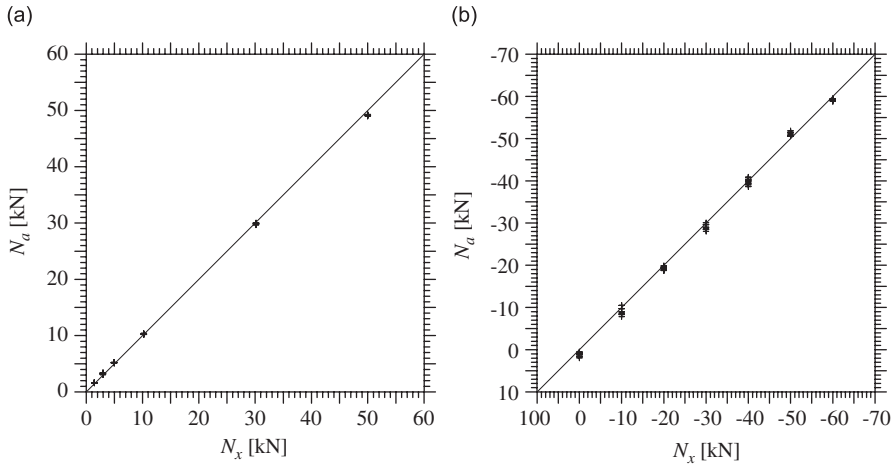

Fig. 8. Comparison between measured (N_x) and estimated (N_a) forces. Tensile (a) and compression (b) vibration tests.

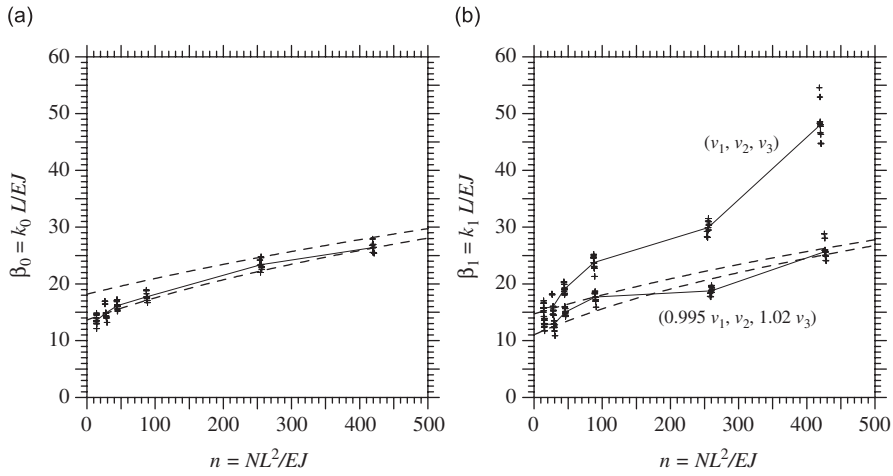

Fig. 9. Tensile vibration tests. End constraint stiffness β_0 (a) and β_1 (b) of the central span versus the tensile force N.

Table 3
Compression vibration tests. Average of the experimental parameters

Test	N_x (kN)	f_1 (Hz)	v_1/v_2	v_3/v_2
1	0.00	31.05	0.612	0.630
2	−10.00	29.42	0.612	0.625
3	−20.00	27.82	0.610	0.622
4	−30.00	26.17	0.607	0.618
5	−40.00	23.96	0.605	0.618
6	−50.00	21.85	0.601	0.612
7	−60.00	20.14	0.599	0.607

Table 4
Compression vibration tests. Experimental and estimated parameters

Test	Experimental data		Estimated parameters			
	λ	$(v_1+v_3)/2v_2$	n_a	N_a (kN)	β_0	β_1
1	4.18	0.621	0.32	1.09	11.5	9.6
2	4.07	0.619	−2.69	−9.26	11.2	9.9
3	3.96	0.616	−5.56	−19.15	11.3	10.0
4	3.84	0.613	−8.49	−29.27	11.5	10.4
5	3.68	0.611	−11.56	−39.84	11.3	10.0
6	3.51	0.606	−14.86	−51.20	11.7	10.6
7	3.37	0.603	−17.18	−59.21	11.8	11.0

with the arbitrary values 0.995 v_1/v_2 and 1.02 v_3/v_2, the corresponding line of Fig. 9 is obtained, which is much closer to the limit (dotted) lines. Hence, identification of boundary conditions is clearly ill conditioned. Analogous results were obtained for beams with different span configurations.

5.2. Compression tests

As for compression tests (Fig. 5), the case $L_s = 500\,\text{mm}$, $L = 2380\,\text{mm}$, and $L_d = 560\,\text{mm}$ is reported in the following. The central beam to be analyzed was given slenderness sufficient to exclude inelastic buckling. Tables 3 and 4 show measured and estimated mean parameters, respectively. Fig. 8b shows a good agreement between measured and estimated loads N_x and N_a for each test performed. Fig. 10 shows the (estimated) variation of the end constraint stiffness β_0 and β_1 of the central span for a decreasing compressive force N. Cross-symbols correspond to single test evaluations and solid lines represent the average of the nine experimental data. The experimental values for β_0, β_1 are far away from the analytical values corresponding to the limits given by Eqs. (33) and (34). Furthermore, the expected reduction of the elastic parameters β_0 and β_1 for decreasing values of N is not confirmed. Nevertheless, the variation of these parameters is quite small and the following mean values will be adopted in next section:

$$\beta_{0,\text{mean}} = 11.5, \quad \beta_{1,\text{mean}} = 10.2. \tag{40a,b}$$

6. Buckling load evaluation

As is known, Newmark gave a good approximation for the critical load of a single span, slender, compressed beam in the form [8,9]

$$N_{\text{cr}\,E} = \chi \frac{\pi^2 EJ}{l^2} \quad \text{where } \chi = \frac{(0.4+\beta_0^{-1})(0.4+\beta_1^{-1})}{(0.2+\beta_0^{-1})(0.2+\beta_1^{-1})}. \tag{41a,b}$$

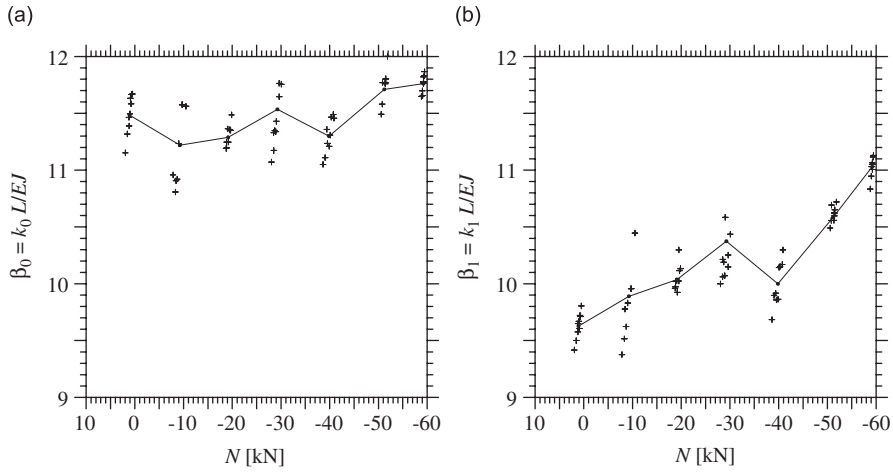

Fig. 10. Compression vibration tests. End constraint stiffness β_0 (a) and β_1 (b) of the central span versus the compressive force N.

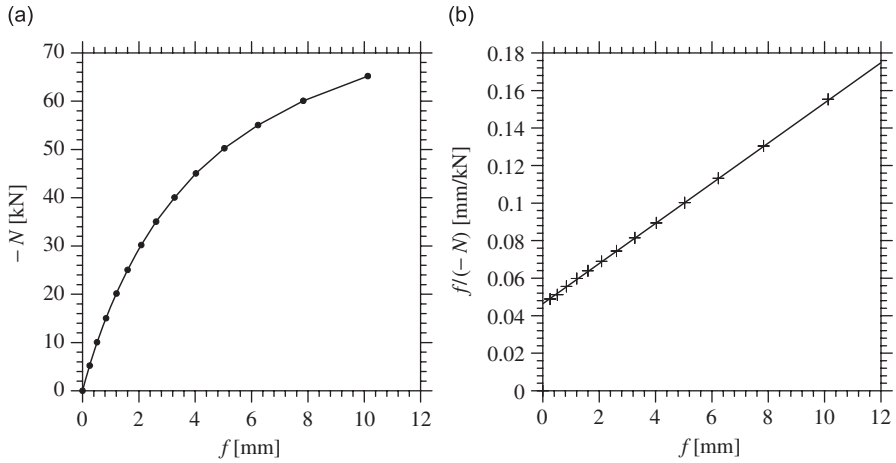

Fig. 11. Force–displacement curve (a) and Southwell plot (b).

Hence, the evaluation of the end constraint stiffness β_0 and β_1 could open the door into the experimental evaluation of the buckling load $N_{\mathrm{cr}\,E}$ by means of vibration tests. In fact, substituting Eqs. (40) into Eqs. (41), the corresponding buckling loads is $N_{\mathrm{cr}\,E,\mathrm{dynamic}} = 96.4\,\mathrm{kN}$.

Aimed at the same goal, the static method proposed by Southwell [9] can profitably be used to obtain an experimental comparison term. In fact, for a beam subjected to a compressive force N (Fig. 11a), this method yields an estimate of the buckling load in the form

$$\frac{f}{(-N)} = \frac{f}{N_{\mathrm{cr}\,E}} + \frac{f_0}{N_{\mathrm{cr}\,E}}, \tag{42}$$

where f is the mid-section displacement and f_0 represents the initial imperfection. Hence, reporting $f/(-N)$ and the same f on the coordinate axes, the inclination of the straight line in Fig. 11b gives the value $1/N_{\mathrm{cr}\,E}$ and the intersection with the $f/(-N)$ axis yields the ratio $f_0/N_{\mathrm{cr}\,E}$. Results of the static test gave $f_0 = 4.32\,\mathrm{mm}$ and $N_{\mathrm{cr}\,E,\mathrm{static}} = 93.1\,\mathrm{kN}$, with an error of about 3.5% with respect to $N_{\mathrm{cr}\,E,\mathrm{dynamic}}$. Therefore, the experimental evaluation of constraint rotational stiffness of a slender beam may represent a significant procedure for the evaluation of the axial buckling load.

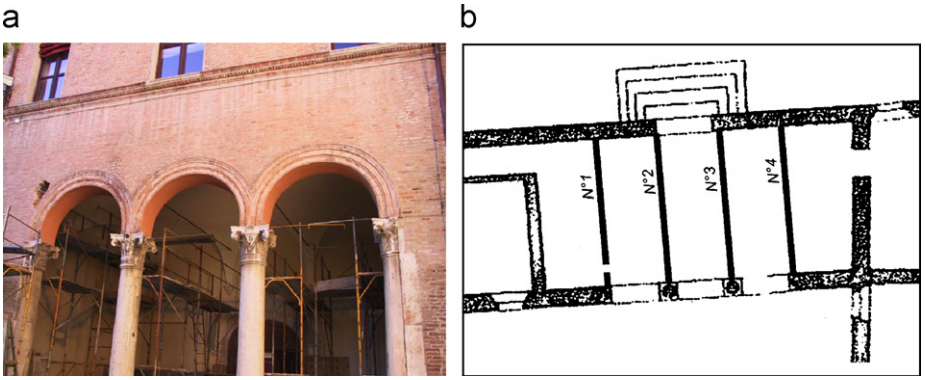

Fig. 12. View (a) and plan (b) of the pavilion vault arcade of Palace Ludovico il Moro in Ferrara.

7. In-situ applications

The first case reported hereafter concerns the 16 century Palace Ludovico il Moro in Ferrara (Italy) which, since the middle of the past century, has housed the civic archaeological museum [5].

In the south, two story, wing of the building, there is a pavilion vault arcade, of $5.50 \times 12.00\,m^2$ resting on two columns and two semi-columns anchored by four forged iron tie-rods having a 30 mm diameter (Fig. 12a). Not long ago, one of tie-beams (named no. 1 in Fig. 12b) exhibited a complete fracture in the proximity of a semi-column giving rise to a 28 mm drift of the abutments (accompanied by quite evident cracks at the vault intrados). The remaining rods were subjected to vibration tests to verify their possible overloading and to assess the tensile force the new rod was to be given. The tie-beams no. 2, 3, 4 showed tensile forces of 86, 90, 81 kN, respectively, and any possible overloading was consequently excluded. Hence, the new tie-rod was given a tensile force of 90 kN by means of a torque wrench acting at the two ends alternatively.

The vibration tests repeated 30 days later, with a more or less similar weather, revealed a reduction of the assigned tensile force of about 50% whereas the adjacent tie-rod showed a reduction of 5 kN.

The second case concerns the 16 century monastery of S. Gregorio Armeno located in the oldest area of Naples (Italy), once occupied by the forum of the Greek-Roman city. The church foundations probably go back to the fifth century A.C. but the present arrangement of the adjacent cloister was deliberated by the Fathers of Trento Council in 1563. The cloister is enclosed by cross vault arcades resting on lavic rock columns. Sudden intrados longitudinal cracks accompanied by out-of-plumb of columns required a timely inspection which showed the disjunction of three contiguous tie-rods (with 30 mm diameter) from the relevant anchor devices. Once again, an accurate reconnaissance of the tensile forces of the surviving tie-rods was necessary to establish the forces the replacement rods were to be given. Actually, different values of the tensile forces allowed to distinguish the original tie-rods from those inserted at the corners of the cloister in later times. The replacement tie-rods were given a relatively small tensile force of 30 kN; in fact, small dead loads were resting on the arcades. At the time being of the present account, it will not be surprising that later vibration tests showed that the new tie-rods had adapted to tensile forces of about 4 kN. A prudent suggestion follows from these experiences: a delayed check of the assigned force should be performed before the tie-rod anchor devices be hidden in the masonry. In short, masonry can unexpectedly resist our conjectures and this is a further reason to recognize that a proper and methodical monitoring is the only way to control its real behavior and, hopefully, to learn from it.

8. Conclusions

An analytical approach was presented, which opens the road into an experimental procedure for evaluating tensile forces in vault or arch tie-rods, or compression forces in slender beams. The equipment is constituted by an impact hammer, three piezoelectric accelerometers, a signal conditioner, and a PC for data acquisition. The inertance function evaluated at three instrumented sections reduces the search for the modal parameters

to the analysis of 1 dof system oscillating with its own natural frequency. Having determined modal parameters for a single oscillation mode, the solution to a transcendental equation yields the axial force together with the rotational stiffness of the end constraints. Laboratory tests showed excellent agreement between the estimated (tensile and compression) forces and the corresponding values measured by a load cell. Stiffness experimental evaluation of the end rotational constraints may open the way into the experimental evaluation of the axial buckling load for slender beam by means of vibration tests.

At the moment, the procedure holds under the condition that no displacement of the beam ends occurs. For instance, this is the case for nonsway frames. A further development is under way to formulate a more general procedure allowing for lateral displacements at the beam ends. Hence, the procedure will be suitable for any slender element of any framed or trussed structure.

Acknowledgments

The present investigation was developed in the framework of two coordinated projects: the Italian Research Program No. 2002081557 coordinated by Prof. Luigia Binda from Polytechnic of Milan and the Research Program FAR 2007 of the University of Ferrara. Financial support of the Italian Ministry of University and Research, and of the University of Ferrara is gratefully acknowledged.

References

[1] S. Briccoli Bati, P. Puccetti, U. Tonietti, Experimental methods for testing the pull tension of chains, in: C. Hallai, P. Kulcsar (Eds.), *Proceedings of the 13th World Conference on Non-Destructive Testing*, Elsevier, Amsterdam, 1992, pp. 1259–1263.
[2] S. Briccoli Bati, U. Tonietti, Experimental methods for estimating in situ tensile force in tie-rods, *Journal of Engineering Mechanics* 127 (12) (2001) 1275–1283.
[3] C. Blasi, S. Sorace, Determining the axial force in metallic rods, *Structural Engineering International* 4 (4) (1994) 241–246.
[4] S. Sorace, Parameter models for estimating in-situ tensile force in tie-rods, *Journal of Engineering Mechanics* 122 (9) (1996) 818–825.
[5] G. Bruschi, G. Nardoni, L. Lanza, F. Laudiero, N. Tullini, G. Mezzadri, S. Tralli, Experimental stress analysis of historical forged tie beams of archaeological museum of Spina in Ferrara, Italy, in: C. Modena, P.B. Lourenço, P. Roca (Eds.), *Proceedings of the Structural Analysis of Historical Constructions*, Vol. 1, Taylor & Francis, London, 2004, pp. 489–497.
[6] S. Lagomarsino, C. Calderini, The dynamical identification of the tensile force in ancient tie-rods, *Engineering Structures* 27 (6) (2005) 846–856.
[7] S. Park, S. Choi, S.T. Oh, N. Stubbs, H.C. Song, Identification of the tensile force in high-tension bars using modal sensitivities, *International Journal of Solids and Structures* 43 (10) (2006) 3185–3196.
[8] Z.P. Bazant, L. Cedolin, *Stability of Structures. Elastic, Inelastic, Fracture, and Damage Theories*, Oxford University Press, Oxford, 1991.
[9] J. Singer, J. Arbocz, T. Weller, *Buckling Experiments: Volume 1, Basic Concepts, Columns, Beams and Plates*, Wiley, New York, 2000.
[10] H. Lurie, Lateral vibrations as related to structural stability, *Journal of Applied Mechanics* 19 (2) (1952) 195–203.
[11] R.H. Plaut, L.N. Virgin, Use of frequency data to predict buckling, *Journal of Engineering Mechanics* 116 (1990) 2330–2335.
[12] L.N. Virgin, R.H. Plaut, Effect of axial load on forced vibrations of beams, *Journal of Sound and Vibration* 168 (3) (1993) 395–405.
[13] M. Baruch, Integral equations for nondestructive determination of buckling loads for elastic bars and plates, *Israel Journal of Technology* 11 (1–2) (1973) 1–8.
[14] A. Segall, M. Baruch, A non-destructive dynamic method for determination of the critical load of elastic column, *Experimental Mechanics* 20 (1980) 285–288.
[15] C.G. Go, Y.S. Lin, E.H. Khor, Experimental determination of the buckling load of a straight structural member by using dynamic parameters, *Journal of Sound and Vibration* 205 (3) (1997) 257–264.
[16] M.J. Jacobson, M.L. Wenner, Predicting buckling loads from vibrational data, *Experimental Mechanics* 8 (10) (1968) 35N–38N.
[17] T. Livingston, J.G. Béliveau, D.R. Huston, Estimation of axial load in prismatic members using flexural vibrations, *Journal of Sound and Vibration* 179 (5) (1995) 899–908.
[18] P.D. Greening, N.A.J. Lieven, Identification and updating of loading in frameworks using dynamic measurements, *Journal of Sound and Vibration* 260 (1) (2003) 101–115.
[19] A.S. Bahra, P.D. Greening, Particularities of Newton's method in space frame force determination utilising eigenpair functions, *Journal of Sound and Vibration* 291 (1–2) (2006) 462–490.
[20] J.E.R. Flores, F.A.C. Viana, D.A. Rade, V. Steffen Jr., Identification of external forces in mechanical systems by using lifecycle model and stress-stiffening effect, *Mechanical Systems and Signal Processing* 21 (7) (2007) 2900–2917.
[21] F.J. Shaker, Effect of axial load on mode shapes and frequencies of beams, *NASA Technical Note (NASA TN D-8109)*, 1975.
[22] B. Klein, Determination of effective end fixity of columns with unequal rotational end restraints by means of vibration test data, *Journal of the Royal Aeronautical Society* 61 (1957) 131–132.

[23] A.L. Sweet, J. Genin, P.F. Mlakar, Vibratory identification of beam boundary conditions, *Journal of Dynamic Systems, Measurement and Control* 98 (1976) 387–394.
[24] Lord Rayleigh, *Theory of Sound*, Vol. I, Dover, New York, 1877 re-issued 1945.
[25] K.F. Graff, *Wave Motion in Elastic Solids*, Dover, New York, 1975 re-issued 1991.
[26] A. Bokaian, Natural frequencies of beams under compressive axial loads, *Journal of Sound and Vibration* 126 (1) (1988) 49–65.
[27] A. Bokaian, Natural frequencies of beams under tensile axial loads, *Journal of Sound and Vibration* 142 (3) (1990) 481–498.
[28] L.N. Virgin, *Vibration of Axially Loaded Structures*, Cambridge University Press, New York, 2007.
[29] P. Morse, K.U. Ingard, *Theoretical Acoustics*, Princeton University Press, Princeton, 1987.
[30] Laboratoire Central des Ponts et Chaussèes, Mesure de la tension des cables par vibration, Méthode d'essai LPC No. 35, 1993.
[31] R. Geier, G. De Roeck, R. Flesch, Accurate cable force determination using ambient vibration measurements, *Structure and Infrastructure Engineering* 2 (1) (2006) 43–52.
[32] G.M.L. Gladwell, *Inverse Problems in Vibration*, second ed., Springer, Berlin, 2004.
[33] W.F. Chen, E.M. Lui (Eds.), *Handbook of Structural Engineering*, second ed., CRC Press, Boca Raton, FL, 2005.
[34] D.J. Ewins, *Modal Testing: Theory and Practice*, Wiley, New York, 1984.
[35] C.M. Harris, A.G. Piersol (Eds.), *Harris' Shock and Vibration Handbook*, fifth ed., McGraw Hill, New York, 2002.